Scanning Electron Microscopy

Volume 1986 | Number 2 Article 9

7-16-1986

Mapping Solid Surfaces with a Raman Microprobe

P. M. Fauchet
Princeton University

Follow this and additional works at: https://digitalcommons.usu.edu/electron

Part of the Biology Commons

Recommended Citation

Fauchet, P. M. (1986) "Mapping Solid Surfaces with a Raman Microprobe," *Scanning Electron Microscopy*: Vol. 1986 : No. 2 , Article 9.
Available at: https://digitalcommons.usu.edu/electron/vol1986/iss2/9

This Article is brought to you for free and open access by the Western Dairy Center at DigitalCommons@USU. It has been accepted for inclusion in Scanning Electron Microscopy by an authorized administrator of DigitalCommons@USU. For more information, please contact digitalcommons@usu.edu.

SCANNING ELECTRON MICROSCOPY/1986/II (Pages 425-435)
SEM Inc., AMF O'Hare (Chicago), IL 60666-0507 USA

0586-5581/86$1.00+05

MAPPING SOLID SURFACES WITH A RAMAN MICROPROBE

P. M. Fauchet

Department of Electrical Engineering
Princeton University, Princeton NJ 08544
Phone: 609 452-4416

(Received for publication March 10, 1986: revised paper received July 16, 1986)

Abstract

By combining an optical microscope with a standard Raman scattering apparatus, information on the structure, composition, homogeneity, and stress state of solids can be obtained with one micron resolution. After a discussion of the advantages and implementation of the technique, we examine specific applications mostly taken from our own work dealing with laser-solid interactions. In particular, we examine the structural modifications produced during laser annealing of semiconductors and laser induced damage of thin films.

Key words: Raman microprobe, laser annealing, laser damage, stress, homogeneity, silicon-on-insulator.

Introduction

The characterization of solids is a field of ever increasing importance. Thanks to advanced techniques such as molecular beam epitaxy, lithography, and laser processing, it is now possible to manufacture complex materials and micron-size structures. The need for novel diagnostic tools that are quantitative, easy to use, and have appropriate spatial resolution is becoming more acute. Raman spectroscopy is a powerful method that has been successfully in use for many years in a laboratory environment. It gives quantitative information on the structure, composition, homogeneity, stress, and other properties of materials. By combining an optical microscope with a standard Raman apparatus, the same information can be obtained with one micron spatial resolution.

The Raman microprobe

In a standard Raman scattering apparatus, a monochromatic laser beam (typically from a continuous wave argon ion laser) impinges on the sample. A small fraction of the incident photons are frequency shifted in the Raman scattering process and reemitted more or less isotropically. A lens is used to collect a fraction of the Raman photons, which are then directed onto a spectrometer. In the spectrometer, photons of different wavelengths are physically separated under the dispersive influence of one or several gratings. A detector is placed at the exit of the spectrometer. The most usual arrangement is to use small slits that pass a narrow wavelength range at a time, and to scan the wavelength, so as to obtain the entire Raman line or spectrum. The detector is a cooled photomultiplier (PMT). Recently, optical multichannel analyzers (OMA) and charge-coupled devices (CCD) arrays have become more popular. A large fraction of the spectrum is then recorded at once on an array of detectors, each small element recording a narrow wavelength range. The data acquisition time is thus greatly decreased. A much larger cost and usually somewhat reduced resolution offset in part the gain in time.

Our Instruments S.A. Raman microprobe is shown schematically in Figure 1. An optical beam, produced by a continuous wave argon or krypton ion laser,

is attenuated and polarized before entering a commercial microscope. The beam is directed onto the objective by a beam splitter and focused to a one micron spot. To avoid heating, we usually keep the power at the sample below 5 mW, except when working with transparent media. Raman photons emitted from the illuminated spot are collected by the same microscope objective, transmitted through the beamsplitter, passed into an analyzer, and sent to the spectrometer. Presently, detection is performed with a PMT in the photon counting mode, and the data are stored by a computer and displayed in real time. The computer controls the wavelength scan and will in the very near future position the sample. Fine absolute positioning is made possible by displaying the image of the surface and of the focused laser beam on a screen. In our experience, illumination of the surface with a somewhat defocused laser beam and examination of the image on the screen is a method of surface characterization nearly as sensitive as high resolution Nomarski optical microscopy.

The background light rejection ratio of the Raman microprobe is comparable to that of a good macro-Raman arrangement, except in the low wavenumber shift region. The accuracy and repeatability of the instrument is 0.1 wavenumbers. The spectral resolution, which is controlled by the slit width, is routinely set at 3 wavenumbers. This represents an optimum compromise between resolution and data acquisition time. Despite focusing the beam to its diffraction limit, highly polarized light can be used, which is useful in some applications.

The physics of Raman scattering

Raman scattering is a process which can take place in any material, gases, liquids, and solids [2]. Therefore, its use is not restricted to solids, and the Raman microprobe may be useful for studying liquids or biological samples. In solids however, lattice vibrations (phonons) scatter off some of the incident photons. The photons thus reemitted are frequency shifted by an amount equal to the phonon energy. This frequency shift is in the 250 to 600 wavenumber range for optic phonons in most semiconductors of technological interest, such as Si or GaAs. Very few photons suffer Raman scattering and thus for the typical laser powers used in our experiments, we detect from one to ten thousand counts per second per frequency channel in a typical Raman line. If a detailed analysis of the Raman line is required, the counting time per channel is 2 to 20 seconds.

Since the Raman process involves the participation of phonons, any factor acting on the phonon properties is measurable. In the simplest experiment, the spectrum is recorded over a wide wavenumber range (say from 200 to 1000 wavenumbers) with a coarse resolution. The position of the observed peaks is then matched against that of the known peaks of various materials. In this way, and by comparing the strength of peaks belonging to different compounds, the composition of an unknown sample can be determined. The crystal orientation can also be determined by using well-established selection rules [4]. The average grain size and shape in polycrystalline materials can also be deduced from high resolution measurements of specific lines. In general, large grain or single crystal material will have narrow and symmetric lines, whereas small grains below 20 nanometers will be characterized by a line that is shifted, broadened, and asymmetric. By comparing the measured line to the line predicted for a given grain size and shape, both size and shape can be obtained [7]. Distinction between crystalline and amorphous phases of any material is easy, since amorphous solids have much broader lines [18]. Strain can also be detected. For example, the peak of most lines shift linearly with applied stress [1]. The magnitude and sign of the stress or strain can thus be measured. An important application is the measure of strain in heterolayers or thin films that are deposited on a substrate which is not lattice matched. Finally, the concentration, the sign (donor or acceptor), and the nature of impurities can be deduced from the modification of the main Raman lines [3], and from the emergence of weak new lines, associated with local vibration modes of the impurity [10]. However, a moderate to high doping is often required before the influence of impurities can be detected. All these properties can also be measured in a layer of variable thickness. Since the absorption coefficient of semiconductors is an increasing function of photon energies above the bandgap, the Raman signal comes from a layer close to the surface whose thickness is imposed by the frequency of the laser. Such depth profiling experiments have been performed successfully in III-V semiconductors using different wavelengths from an argon ion laser [31].

The advantages of the Raman microprobe should now be rather obvious. Its spatial resolution is comparable to that of an optical microscope and three dimensional mapping is possible with depth profiling. It is easy to implement: there is no need for special sample preparation, or use of vacuum chambers. It gives access to quantitative information on structural properties of the sample which are often difficult to obtain otherwise. Finally, and most importantly, it is a non-destructive tool. Other techniques, such as scanning electron microscopy (SEM), transmission electron microscopy (TEM), and optical microscopy, do not measure structural properties so thoroughly and easily, although they all have specific advantages, for example in resolution (SEM, TEM) and in cost (optical microscope). The Raman microprobe belongs to a family of emerging tools that includes the scanning acoustic microscope [30] which are starting to have an impact on the field of characterization of small structures. Note that after suitable modifications of our present system, it should be possible to have a scanning Raman microscope.

Applications in the field of laser processing

We have chosen to illustrate the power of the Raman microprobe by reviewing applications in the field

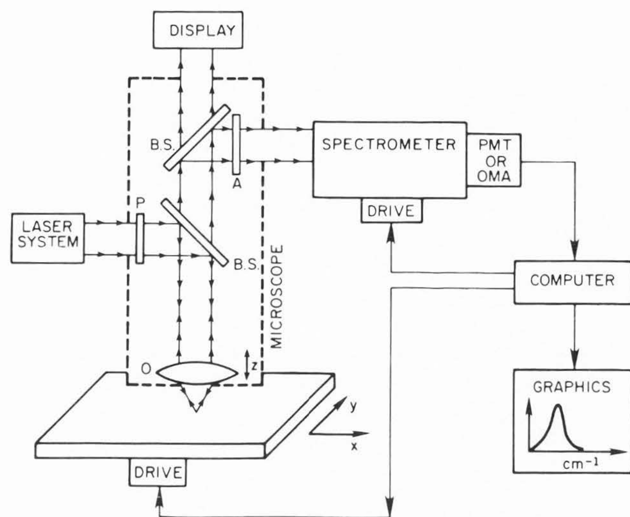

Figure 1

Block diagram of the Raman microprobe. The probe laser beam is focused through the objective 0 to a one micron spot on the sample surface. The backscattered Raman signal is collimated by the same objective and analyzed by a double-1 meter spectrometer. The standard optical microscopic image of the surface appears on the display.

of laser processing of solids. Most of our work and a large fraction of the literature on the use of the Raman microprobe have been in that field. High power lasers can be focused to micron-sized spots and thus modify the structure and composition of solids on that scale.

Laser annealing

In this section, we review several publications dealing with the uses of continuous wave lasers to recrystallize amorphous semiconductor layers. Several groups, including us, have measured the stress variations in laser-recrystallized silicon-on-insulator (SOI) structures [21,32]. Typically, an oxide layer is deposited on a silicon wafer which covers the entire surface except for small protruding areas. These areas are called seed regions and are made on small epitaxial silicon. Amorphous silicon is then deposited on top of the wafer and subsequently recrystallized by scanning a focused argon ion laser beam. The role of the seed regions is to initiate crystallization. The material thus obtained is polycrystalline with large grain sizes (much larger than one micron). Similar results can be obtained by rapid thermal annealing (RTA). Here, the laser is replaced by a strip heater under which the sample is slowly translated [29]. With laser annealing, it has been observed that there is an increase in tensile stress away from the seed region, typically from $3x10^9$ to $5x10^9$ dyne/cm^2, obtained from the shift of the Raman line. A small variation with depth has been reported by Zorabedian and Adar [32]. In contrast, we have observed in the RTA silicon a constant stress smaller than $4x10^8$ dyne/cm^2, comparable to resolution in that particular experiment. A complete explanation of these observations will be published elsewhere.

Nakashima and coworkers [27] have used an argon ion laser to recrystallize fine lines in polycrystalline silicon layers deposited on (100) silicon substrates and amorphized by ion-implantation. Figure 2 shows the Raman microprobe data obtained by scanning the probe laser across the recrystallized lines. At high power (7 W) epitaxial regrowth took place from the substrate indicating that the entire layer was melted. At low power (3 W) partial recrystallization took place, indicating that the liquid/solid interface never reached the substrate. The material is polycrystalline and the grain

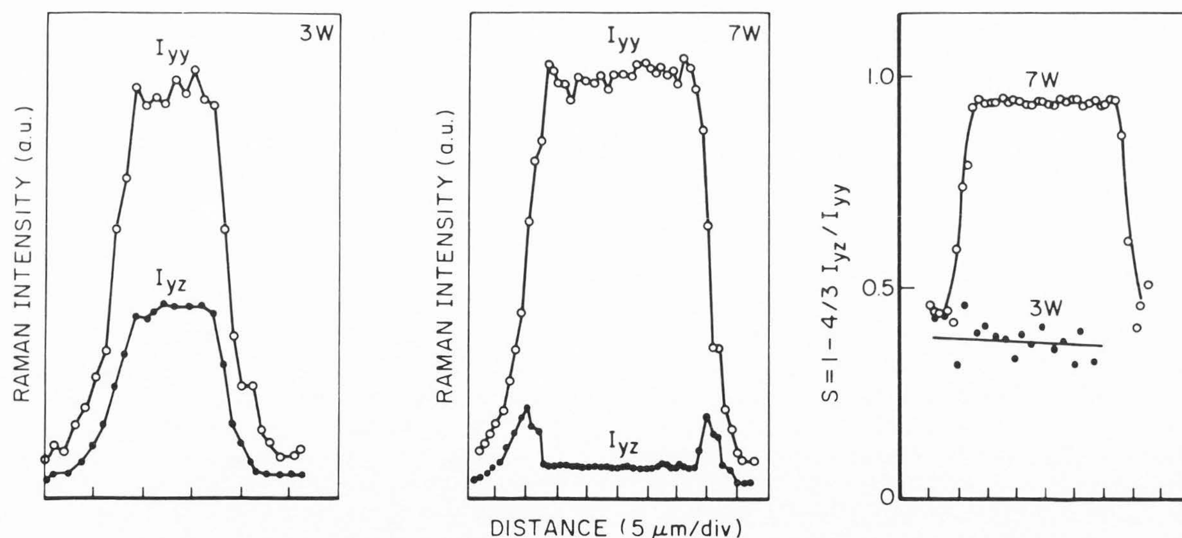

Figure 2 Polarization microprobe measurements across a $\sim 25\ \mu m$ laser recrystallized poly-Si film on <100> substrate. At 3 watts, epitaxy did not take place from the substrate, while at 7 watts it did, as indicated by the ratio of allowed (I_{yy}) over forbidden (I_{yz}) intensities. After Nakashima et al., ref. 27.

orientation is not uniform. This analysis comes from the comparison of the Raman intensity with incident and scattered photons having parallel (Iyy) and perpendicular (Iyz) polarizations. For (100) silicon, Iyz should be equal to zero. Thus, at low power, the crystal orientation is not purely (100): the material is made of many grains with nonuniform orientations. The quantity S quantifies this conclusion. For single crystal, S=1, while for randomly oriented grains, S=0. At low power, the grains are not totally randomly oriented, as can be expected from the dependence of growth velocity on orientation [11].

In a related study, a similar polarization-selective Raman technique has been used to measure the orientation of large grains with respect to the substrate [16,17]. Abrupt changes in grain orientation have been observed across grain boundaries, indicating a loss of epitaxy from the seed to the silicon on the oxide. Others have used the Raman microprobe to investigate the quality of liquid phase epitaxy after pulsed laser annealing of ion-implanted, amorphous silicon and gallium arsenide [24,28].

Pulsed laser melting of thin polycrystalline films

In this section, we report on our work concerning the changes in crystallinity, stress, and homogeneity of thin polycrystalline films of silicon on insulators irradiated by intense and short laser pulses. These films were grown by low pressure chemical vapor deposition (LPCVD) at 625 °C. They are 1 micron thick, have a columnar structure, and are under tensile stress due to the difference in the thermal expansion coefficient of silicon and the fused quartz substrate. Picosecond pulses from a Nd:YAG laser are focused to a 150 micron spot, and the intensity at each of the three wavelengths used, 1064, 532, and 355 nanometers, is adjusted to produce molten spots of equal sizes. The processed areas are first examined by high resolution Nomarski optical microscopy, to determine the extent and character of the surface transformation. We then record the Raman spectra, in and around the transformed area. The Raman line is characterized by four major parameters: the number of counts at the peak of the line, the frequency shift with respect to the unprocessed sample, the full-width half-maximum of the line, and the asymmetry of the line, defined by the ratio of the half-width half-maximum (HWHM) on the low wavenumber side to the HWHM to the high wavenumber side. Figure 3 shows high resolution spectra of the main Raman line of crystalline silicon and of the polycrystalline films under study. Figure 4 consists of three sets of data, taken after irradiation at 1064, 532, and 355 nm, respectively [8]. In addition to the four parameters just mentioned, we show schematically the cross-section of the film at and around the irradiated spot. Note first the difference between the scale at 1064 nm, and 532 or 355 nm. At 1064 nm, there has been almost complete vaporization of the silicon film in the central region of the illuminated spot. In region 1, which is at the border of the crater, we find silicon grains larger than 30 nm under roughly the same stress

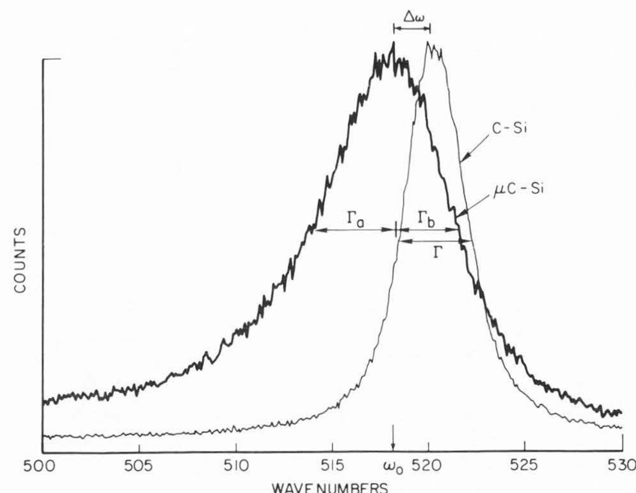

Figure 3

Optic phonon Stokes line of single crystal silicon (fine line) and of polycrystalline silicon thin film (thick line). With the standard operating parameters of our instrument, $\omega_o = 520\ \mathrm{cm}^{-1}$, $\Gamma \simeq 3.8\mathrm{cm}^{-1}$, and $\Gamma_a/\Gamma_b \simeq 1$, for crystalline silicon, and $\omega_o \simeq 518.5\mathrm{cm}^{-1}$, $\Gamma \simeq 9\mathrm{cm}^{-1}$, and $\Gamma_a/\Gamma_b \simeq 1.4$ for the polycrystalline silicon thin films. In these films, the exact parameters of the Raman line are not perfectly identical everywhere (for example, ω_o varies from 518.5 to 519 cm^{-1} over large distances). These variations reflect stress and homogeneity changes in the film itself.

as the original film. In region 2, we find an excess material, probably forced out by surface tension gradients. The very large number of counts in that region confirms what we observed under the optical microscope. If the film had been thicker than one micron, the addition of extra silicon layers would not have changed the Raman line intensity because the penetration depth at the probing wavelength is nearly equal to one micron. In the part of region 2 that is closer to the unperturbed material of region 3, the tensile stress is increased by $3.5\mathrm{x}10^9$ dyne/cm^2. A similar experiment performed with a 100 ns-long train of 20 pulses each having a duration of 100 ps yielded qualitatively different results: no crater was formed, and there was a region outside the visibly processed area which was under excess stress. The damage observed with the single picosecond 1064 nm pulse comes from the very nonlinear absorption processes that take place during illumination [5]. The 1064 nm infrared photons are initially weakly absorbed in the silicon. However, the intensity is so high that free carrier absorption and possibly two-photon absorption contribute efficiently to a temperature rise in the central region where the intensity is maximum. The bandgap then decreases, absorption becomes more efficient, the temperature rises even faster, and we have a catastrophic runaway leading to melting and vaporization in the central

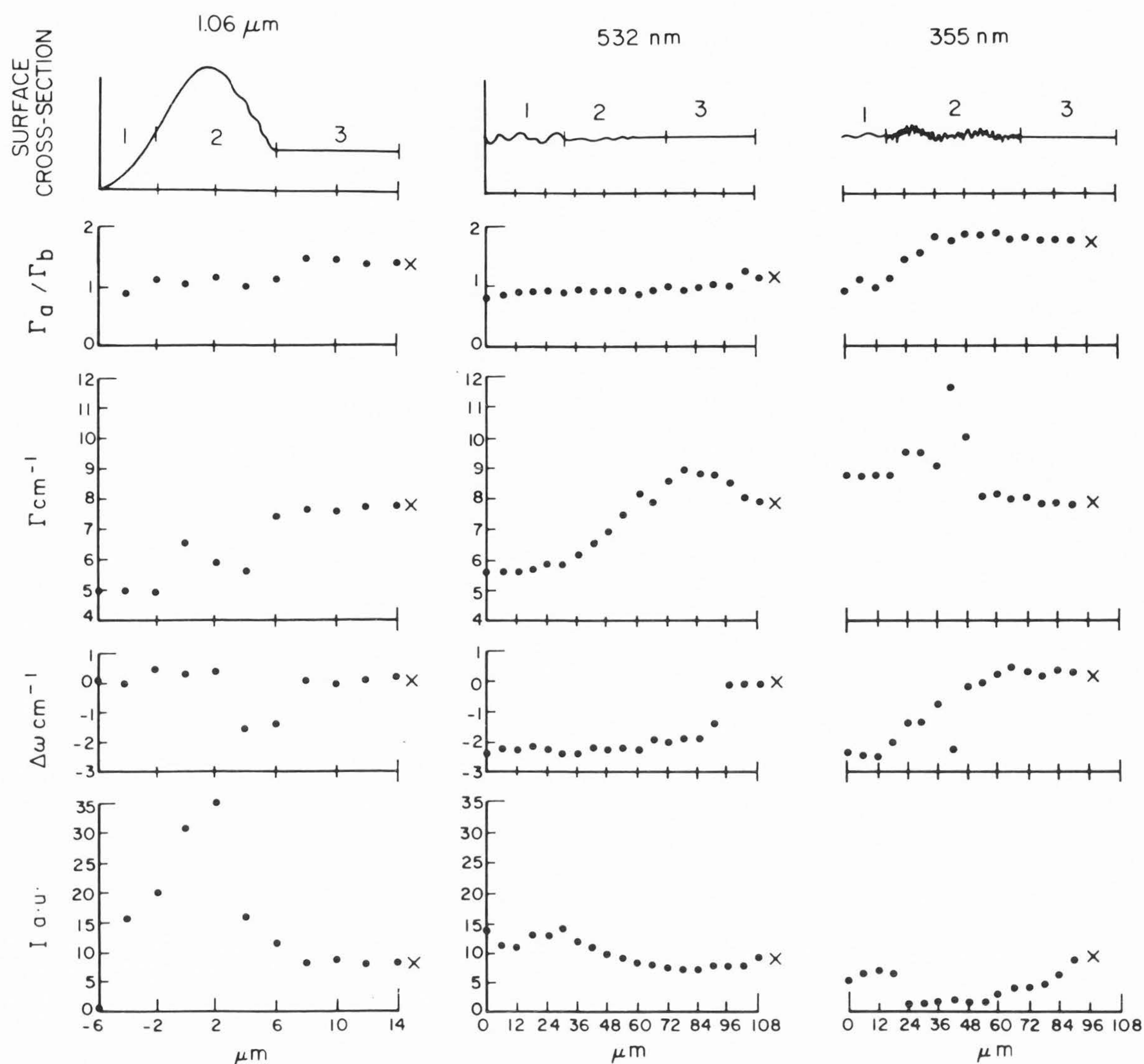

Figure 4. A B C

A: Morphology and Raman results at the edge of the damage crater for a spot irradiated with 1.06μm radiation. Moving in the negative direction is toward the center of the spot while positive distances are toward the unprocessed SOI which is marked with an x.

B,C: Morphology and Raman results for spots irradiated with 532 nm and 355 nm radiation moving from the center of the spot to the unprocessed SOI. Note that there are some differences in the unprocessed SOI quality between the regions exposed to 355 nm and 532 nm light which were separated by a few centimeters.

region. On the outside, the beam intensity was never sufficient to trigger the runaway and we are left with a sharp boundary between vaporized and essentially unheated material. In contrast, each pulse in the 100 ns train is not intense enough to create many free carriers or two photon absorption, even less the runaway. However, each pulse contributes to a modest temperature increase, which is softened by diffusion between pulses, but remains enough to increase the coupling of the next pulse. The band-to-band absorption coefficient for the photons in the next pulse is then increased and toward the middle of the train, resembles the absorption coefficient at shorter wavelength (for example, 532 nm) but lower temperature.

Our Raman measurements after irradiation by a single 30 ps/532 nm pulse or by a train of 100 ps pulses at 1064 nm are similar for the reasons explained above. Referring to Figure 4B, we observe in the central region 1 large microcrystals (>30 nm) that are under considerable tensile stress (6×10^9 dyne/cm^2). The surface appears rough but the Raman line is quite uniform across that region. In this region, thorough melting of the layer has taken place, and larger grains have been formed during recrystallization. The excess stress may

be explained by the somewhat higher density of crystalline (or large grain polycrystalline) silicon compared to SOI. In region 2, the stress becomes heterogeneous because the entire layer has not been melted. In region 3, which is beyond the visible boundary between processed and virgin material, there is a gradual recovery of the Raman line, which is complete after 20 microns. Eighteen microns beyond region 2, the stress relaxes rapidly, at a rate of $5x10^8$ dyne/cm^2 per micron. The grain size also recovers at the same time as the stress becomes equal to that of the virgin SOI. Although a detailed explanation of these observations is not available yet, we believe that heat diffusion in the layer away from the molten material, coupled to the contraction of the central region will explain our findings. In support of this interpretation, we offer two additional results [12]. First, in similar SOI films, we produced an interference pattern by overlapping two equal-intensity beams having a small angle between them. The intensity is thus modulated in the sample. We adjusted the beams so as to exceed melting threshold at the constructive interference (CI) points. No power is flowing directly from the beams into the sample at the destructive interference (DI) points. The period of the pattern was approximately 5 microns. Figure 5 shows the Raman line before illumination, and after illumination on stripes of constructive and destructive interference regions. The line observed after illumination is different from that of the virgin material and the difference between curves b and c is minor. The symmetrization and narrowing of the line indicates a transformation that increases the tensile stress by $5x10^9$ dyne/cm^2 and the grain size beyond the detection limit [7]. In the DI region, the modifications have been produced because heat transport took place from the CI regions. In this particular case, the excess energy in the CI stripes was large enough to melt almost thoroughly the DI stripes. The larger small wavenumber tail in the DI regions, which indicates slightly smaller grain sizes and perhaps also slightly increases inhomogeneity, is the only difference between the two types of regions. In a second set of experiments, we repeated each experiment on wafers. In the single beam illumination case, we do not observe much change on top of the melted spot. In the two beam case, although we were able to clearly distinguish between molten and unmelted stripes with an optical microscope, the Raman line exhibited no change and in fact remained essentially undistinguishable from that of the virgin wafer. With the wafers, heat can flow perpendicular to the surface (where the gradient is maximum) and epitaxy always takes place from the single crystal wafer.

Finally, Figure 4 presents the major features of the Raman line after irradiation of the SOI samples with single 355 nm picosecond pulses. The material in region 1 is microcrystalline with large grains and is under a heterogeneous stress having an average value of $6x10^9$ dyne/cm^2. In region 2, we find small grains still under a heterogeneous stress that relaxes slowly at an average rate approximately equal to 10^8 dyne/cm^2 per micron. In region 3, the top layer is made of amorphous silicon while the rest of the film looks identical to the unprocessed film. The presence of the amorphous layer is confirmed by the emergence of a very weak and broad peak around 480 wavenumbers and by the reduced amplitude of the polycrystalline peak. At 355 nm, light is absorbed within 20 nm of the surface. Only the topmost layer melts. Because of the shallowness of the molten region, regrowth is so fast that the maximum growth velocity for crystalline silicon is exceeded. That layer solidifies in the amorphous phase. Similar amorphization has been observed on wafers [19] but this is the first time it has been produced in thin films. In the center of the illuminated spot, the thickness of the molten layer is much larger because more energy is deposited in the solid, and the regrowth velocity does not exceed the maximum growth velocity for crystalline silicon. That thicker layer solidifies in the crystalline phase. However, due to the large gradients during melting, the material is left under a very inhomogeneous stress which is apparent from the very large FWHM of the Raman line. In region 3, the thickness of the amorphous layer decreases at a rate of 1 nm per micron. This number is obtained by recording the recovery of the amplitude of the polycrystalline line. Since the absorption coefficient of amorphous silicon at the probe wavelength is known, the amplitude of the line will decrease by a calculable amount for any given thickness of the amorphous layer. Finally, we observe no modification of the Raman spectrum beyond the limit between visibly transformed material and virgin SOI.

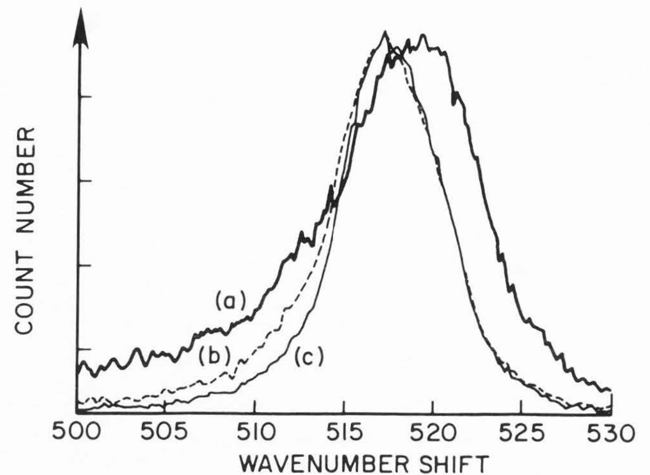

Figure 5

Stokes line of Si in a polycrystalline film on insulator. (a) virgin material; (b) region of destructive interference; (c) region of constructive interference.

Laser induced damage in thin films

The nature of single shot and multiple shot laser-induced damage in thin films, such as those used for optical coatings, remains a source of much controversy. In the broadest sense, damage is defined as any permanent alteration of an optical component that modifies

Figure 6

Spectra taken around an isolated ~1 micron damage-site formed on a polycrystalline silicon film by a single 40 ps/1064 nm laser pulse at damage threshold. The spectra are taken (from top to bottom) on top of the damage site, on its edge, 2, 5, and 9 microns away, and on virgin, unirradiated material. High resolution Nomarski microscopy suggests that the surface remains unaltered except right at the ~1 micron damage site. The amorphous-like shoulder at 495 cm^{-1}, quite apparent in the virgin material, reappears starting at 5 microns away. This shoulder indicates the presence of a relatively large fractional volume of highly distorted material, presumably the grain boundary material. Closer to the damage site, the average grain size has increased, perhaps following melting and recrystallization, and the material is under considerable stress. This extra stress relaxes away from the damage site but has not recovered to the value in the virgin film even after 9 microns.

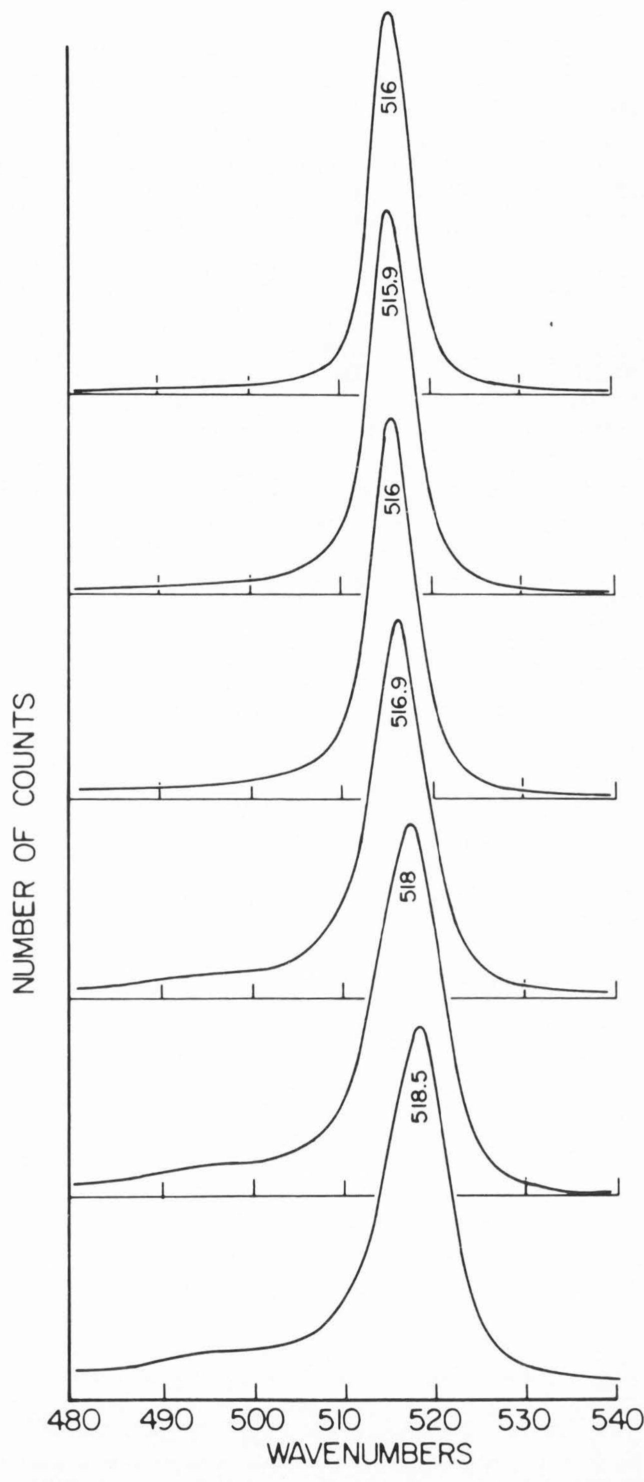

its properties in a deleterious way. In present day technology, the weakest link in any optical system is the coatings. Two forms of damage are important. First, there is the catastrophic vaporization produced by illumination with single pulses that are too intense [20]. Second, there is the gradual degradation of components under repeated illumination [23], which may culminate with a more catastrophic process such as vaporization. The first type of damage is not fully understood yet but it is widely accepted that it is associated with defects that are present in the film. The second type of damage, which is encountered not only in coatings, but also in bulk solids, and not only in transparent media, but also in metals, is not understood presently. There has been a suggestion that thermal cycling of the material during each shot may trigger plastic deformations [26] which in turn roughen the surface and thus increase the absorption. This hypothesis has been proposed for metals but it is conceivable that a similar mechanism could explain the so-called "optical fatigue" phenomenon observed in dielectrics. We have embarked on an experimental program aimed at uncovering the mechanisms of laser-induced damage with the help of the Raman microprobe. If damage is first initiated at very localized areas, the good spatial resolution of the microprobe is essential.

In the first experiments [13], we demonstrated the validity of our approach by performing experiments in SOI films, irradiated at 1064 nm. At these wavelengths, the absorption is initially very weak and the film is essentially transparent, very much like a real coating. The advantage of performing the first experiments in SOI is that SOI is rather well understood and characterized, which is not the case with most optical coatings. Single 40 ps/1064 nm pulses just at damage threshold were focused to a 150 micron spot. High resolution Nomarski optical microscopy revealed a few randomly distributed "wormlike" damage areas 1 to 2 microns in size. The spectra of Figure 6 were taken, from top to bottom, at the center of one isolated damage site, on the edge, 2, 5, and 9 microns away, and on virgin material. The random distribution of damage sites indicates that they are associated with minute imperfections in the film, in agreement with the accepted models.

After damage, the material displays good crystalline properties (narrow line = good homogeneity, symmetric line = large grain size) but is under considerable stress (10^{10} dyne /cm^2). The amorphous like shoulder at 490 wavenumbers, present in the virgin film, is not observed here. We have identified this shoulder with disordered material at the grain boundaries. Its disappearance is another proof of the increase in grain size (larger grain sizes = fewer boundaries). Away from the damage site, where optical microscopy reveals no alteration, the Raman line takes more than 10 microns to recover. This long range relaxation has been verified many times and its interpretation follows the same line as in the discussion of the previous section. From the technological viewpoint, it means that there are now several rather large areas of the film that have been altered. If a second pulse is focused on the same spot, even if its intensity is reduced, further damage is expected to occur because of the film degradation.

In a second experiment [13], many identical laser shots were incident on the SOI. Each shot was at one-half single shot damage threshold (defined as the intensity at which no surface alteration was observed after one shot). Figure 7 shows the Raman line inside and outside a 100 microns heterogeneously damaged area produced by 600 shots. The surface appears to be a dense packing of "wormlike" features. At the edge of the area, there is a smoother annular region. In the center, where damage is heavy, the surface is very distorted and large variations in stress are observed. In the smooth annular region, the stress becomes more uniform, but the FWHM of the Raman line increases, indicating that only a fraction of the film thickness has been melted. At the visible boundary (x = 0), the line is abruptly altered, but still takes 20 microns to fully recover. The wavelength of the probe laser was changed in an attempt to observe any large change with depth. No statistically significant modification of the Raman line was observed, which indicates that any depth variation must be modest.

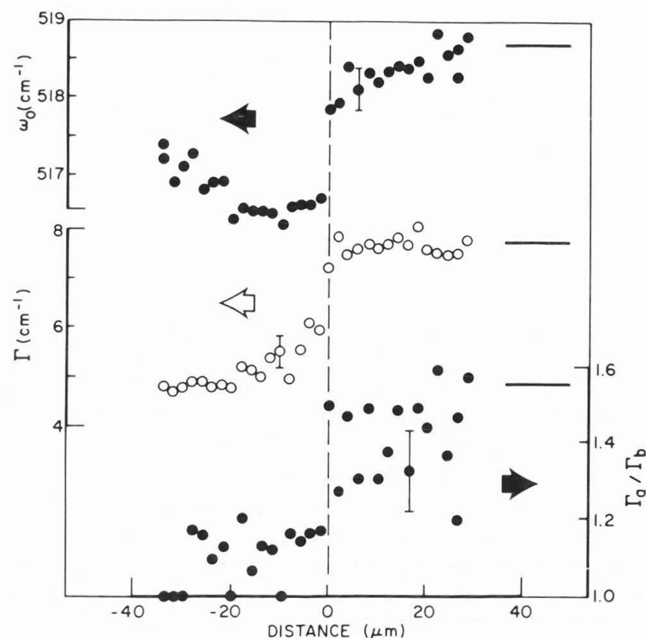

Figure 7

Parameters of the Raman line around a large heterogeneously damaged area formed by repeated illumination (600 shots) at one-half single shot damage. The dashed line indicates the boundary between damaged (left) and undamaged (right) regions as defined by high resolution Nomarski microscopy. The full lines on the right show the parameters of the virgin polycrystalline film. Beyond the visible boundary, it takes $\gtrsim 20$ microns for the Raman line to fully recover. (Note however that Γ seems to recover immediately). Inside the damaged region, we observe different parameters depending upon the smoothness of the surface. In the center, the surface is rough and $\omega_o \sim 517 cm^{-1}$ and $\Gamma \simeq 5 cm^{-1}$. Around the edge, the surface is smoother and $\omega_o \lesssim 516.5 cm^{-1}$ and $\Gamma \sim 5.5 cm^{-1}$.

In Figure 8, we plot the parameters of the Raman line in and around single-shot (■) and multiple-shot (•) damage sites. In general, closer to the damage sites, the FWHM, the peak frequency, and the asymmetry all become smaller. The full line results from a calculation which includes the effects of grain size on the Raman line [7], but neglects the influence of stress. Obviously, the laser-irradiated material is under considerable stress. We also note that the FWHM,the peak frequency, and the asymmetry seem to become smaller on areas damaged by a single laser shot than on areas damaged after multipulse illumination. This difference may indicate that complete melting takes place with single pulses, leading to regrowth with larger grain size under larger tensile stress, whereas with multiple exposure, the material fails heterogeneously and does not undergo thorough melting. This point deserves further study.

The experiments performed on SOI are now being repeated on titania and zirconia thin films, as well as on anti-reflection and high-reflection multilayer structures made of titania, zirconia, and silica [14]. After illumination of a 662 nm thick titania film on silica by several high power 532 nm/ 30 ps laser pulses, we have observed a shift in the intense 142 wavenumbers Raman line of anatase. Our present interpretation of these data is that a stress variation has been induced by the laser. Another group has recently obtained similar results which they also explained in terms of laser-induced stress [15]. More experiments are under way. It already appears that as expected, the Raman microprobe is a promising tool to detect, characterize, and ultimately understand laser-induced damage.

Other applications

For completeness, we list here several other examples of the use of the Raman microprobe to characterize laser-processed materials. The Raman microprobe

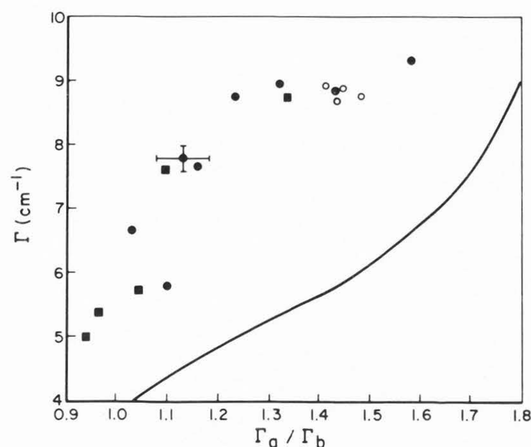

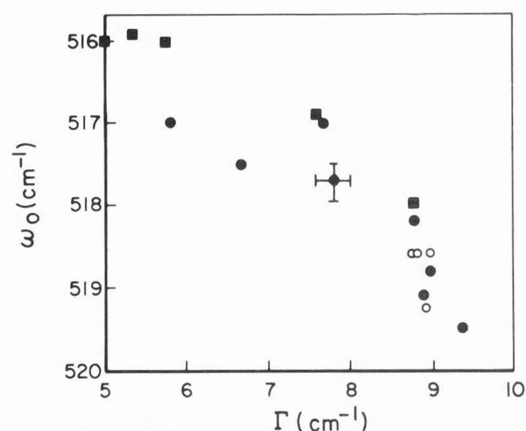

Figure 8

Parameters of the Raman line at various locations in and around single-shot (■) and multishot (•) damage side, and in virgin polycrystalline silicon films (O). The full line, which accounts for variations in the grain size only, does not agree with the data. The ω_o vs Γ data follow a line that actually curves in the opposite direction from that predicted by theory. The stress variations dominate the changes in the Raman line. When ω_o, Γ and Γ_a/Γ_b are small, the material is made of large grains, and is under large and homogeneous tensile stress. Note that the results on single-shot damage sites tend to show a larger and more homogeneous stress.

has been used to observe formation of tungsten silicide after laser-induced chemical vapor deposition of 8 microns wide by 20 nanometers thick tungsten lines on silicon [9]. Refractory metal silicides are very attractive for very large scale integration (VLSI) technology and this study demonstrates that Raman microscopy can provide unique information in a nondestructive fashion and with sufficient resolution for monitoring chip processing and testing VLSI devices. In a very recent study, the same focused argon ion laser beam used to grow Si/Ge lines acted as an in situ, real time probe for a Raman microprobe arrangement [22]. We have also employed the Raman microprobe to study variations in structural properties across periodic (1 to 10 microns) surface undulations or ripples produced by pulsed laser illumination of semiconductors, by explosive crystallization of amorphous films, and by laser-assisted chemical vapor deposition of films containing silicon and carbon [12]. Finally, we should list briefly some other interesting applications of the Raman microprobe: characterization of small silicon devices [6], and detection of minute inclusions within a transparent matrix [25]. In the second example, a long working distance objective was employed to identify a mercuric oxide stain on a silver connector through 3 millimeters of glass. We are also involved with the microcharacterization of epitaxial layers of semiconductors on semiconductors or fluorides.

Conclusion

The Raman microprobe is now several years old. More and more researchers are becoming aware of its potential, as is evident from the published literature. In this review, we have highlighted applications in the field of solid characterization, and more precisely, of laser-processing of solids. We believe that with some minor modifications, such as the use of detector arrays and the transformation of the microprobe into a scanning microscope, it will find applications in many fields, including in the semiconductor processing line.

Acknowledgements

I acknowledge the contributions of I.H. Campbell and F. Adar. This work was supported by the National Science Foundation and IBM.

References

1. Anastassakis, E., Pinczuk, A., Burstein, E., Pollak, F.H., Cardona, M. (1970) "Effect of Uniaxial Stress on the Raman Spectrum of Silicon," *Solid State Commun.*, **8,** 133-138.
2. Anderson, A. (ed.) (1971) *The Raman Effect*, Marcel Dekker Inc., New York.
3. Balkanski, M. (1982) "Optical Properties due to Phonons," in *Handbook on Semiconductors,* vol. 2, Moss, T.S. (Series Ed.), Balkanski, M. (Volume Ed.), Chapter 8, North-Holland, Amsterdam.
4. Birman, J.L. (1982), "Lattice Dynamics-Phonon Symmetry and Selection Rules," in *Handbook on Semiconductors,* vol. 1, Moss, T.S. (Series Ed.), Paul, W. (Volume Ed.) Chapt. 2, North Holland, Amsterdam.
5. Boggess, T.F., Bohnert, K.M., Mansour, K., Moss, S.C., Boyd, I.W., Smirl, A.L. (1986), "Simultaneous measurement of the two-photon coefficient and free-carrier cross-section above the bandgap of crystalline silicon," *IEEE Quantum Electron.*, **QE-22**, 360-368.

6. Brueck, S.R.J., Tsaur, B-Y, Fan, J.C.C., Murphy, D.V., Deutsch, T.F., Silversmith, D.J. (1982), "Raman Measurements of Stress in Silicon-on-Sapphire Device Structures," *Appl. Phys. Lett.*, **40**, 895-898.

7. Campbell, I.H., Fauchet, P.M. (1986), "The effects of microcrystal size and shape on the one phonon Raman spectra of crystalline semiconductors," *Solid State Commun.*, **58**, 739-741.

8. Campbell, I.H., Fauchet, P.M., Adar, F. (1986), "Properties of thin films after focused beam processing," in the Materials Research Society Proceedings Series, Symposium C - Semiconductor on insulator and thin film transistor technology," Materials Research Society, Pittsburgh, PA, in press.

9. Codella, P.J., Adar, F., Liu, Y.S. (1985), "Raman Microprobe Analysis of Tungsten Silicide," *Appl. Phys. Lett.*, **46**, 1076-1078.

10. Contreras, G., Cardona, M., Compaan, A. (1985) "Vibrational Local Mode of Al-Implanted and Laser Annealed Ge," *Solid State Commun.*, **53**, 857-859.

11. Cullis, A.G. (1983), "Ultra-high speed solidification and crystal growth in transiently molten semiconductor layers," in *Laser-Solid Interactions and Transient Thermal Processing of Materials,* Narayan, J., Brown, W.L., and Lemons, R.A. (eds.), North-Holland, New York, pp. 75-82.

12. Fauchet, P.M. (1986), "Raman microprobe analysis of laser-induced microstructures," in *Energy Beam-Solid Interactions*, and *Phase Transformations* Kurz. H., Olson, G.L. and Poate, J.M. (eds.), Materials Research Society, Pittsburgh, PA, 149-154.

13. Fauchet, P.M., Campbell, I.H., Adar, F. (1985), "Long Range Material Relaxation After Localized Laser Damage," *Appl. Phys. Lett.*, **47**, 479-481.

14. Fauchet, P.M., Campbell, I.H., Adar, F. (1986), "Detection of laser damage by Raman microscopy," *Proceedings of the XVIIth Annual Symposium on Optical Materials for High Power Lasers*, NBS Special Publications, in press.

15. Friedrich, D.M., Exarhos, G.J. (1986), "Raman microprobe of laser-induced surface regions in $Ti0_2$ and $Zr0_2$ coatings," in *Proceedings of the XVIIth Annual Symposium on Optical Materials for High Power Lasers*, NBS Special Publications, in press.

16. Hopkins, J.B., Farrow, L.A., Fisanick, G.J. (1984), "Raman Microprobe Determination of Local Crystal Orientation in Laser Annealed Silicon," *Appl. Phys. Lett.*, **44**, 535-537.

17. Hopkins, J.B., Farrow, L.A. (1986), "Raman microprobe determination of local crystal orientation," *J. Appl. Phys.*, **59**, 1103-1110.

18. Lannin, J.S. (1984) "Raman Scattering of Amorphous Si, Ge, and Their Alloys," in *Semiconductors and Semimetals,* Vol. 21B, Willardson, R.K., Beer, A.C. (Series Ed.), Pankove, J.I. (Volume Ed.) Chapt. 6, Academic Press, 159-195.

19. Liu, P.L., Yen, R., Bloembergen, N., Hodgson, R.T. (1979), "Picosecond laser-induced melting and resolidification morphology on Si," *Appl. Phys. Lett.*, **34**, 864-866.

20. Lowdermilk, W.H., Milam, D. (1981), "Laser-Induced Surface and Coating Damage," *IEEE J. Quantum Electron.*, **QE-17**, 1888-1903.

21. Lyon, S.A., Nemanich, R.J., Johnson, N.M., Biegelsen, D.K. (1982) "Microstrain in Laser-Crystallized Silicon Islands on Fused Silica," *Appl. Phys. Lett.*, **40**, 316-318.

22. Magnotta, F., Herman, I.P. (1986), "Real-time Raman microprobe analysis during direct-laser writing of silicon and silicon-germanium alloy microstructures," presented at the Materials Research Society, Pittsburgh, PA, 1985 Fall Meeting, Symposium D. Boston, MA.

23. Merkle, L.D., Bass, M., Swimm, R.T. (1983), "Multiple pulse laser-induced bulk damage in crystalline and fused quartz at 1.064 and 0.532 μm," *Optical Engineering*, **22**, 405-410.

24. Morhange, J.F., Kanellis, G., Balkansi, M. (1980), "Raman Spectroscopy of Amorphous-Crystalline Phase Transition Induced by Laser Annealing," *J. Phys. Soc. Japan*, **49**, suppl. A, 1295-1298.

25. Muggli, R.Z., Andersen, M.E. (1985), "Raman Micro-Analysis of Integrated Circuit Contamination," *Solid State Technol.*, **28**, 287-291.

26. Musal, H.M. (1979), "Thermomechanical stress degradation of metal mirror surfaces under pulsed laser irradiation," in NBS Special Publication **568**, pp. 159-173.

27. Nakashima, S., Inoue, Y., Mitsuishi, A. (1984), "The Evaluation of the Crystallinity of Laser-Annealed Polycrystalline Silicon-on-Silicon Structures by Raman-Microprobe Polarization Measurements," *J. Appl. Phys.*, **56**, 2989-2992.

28. Nisim, Y.I., Sapriel, J., Oudar, J.L. (1983), "Microprobe Raman analysis of picosecond laser annealed implanted silicon," *Appl. Phys. Lett.*,**42**, 504-506.

29. Pfeiffer, L., Celler, G.K., Kovas, T., Robinson, McD., "Suppression of Low angle grain boundaries in seeded thick Si films recrystallized between $Si0_2$ layers," *Appl. Phys. Lett.*, **43**, 1048-1050.

30. Quate, C.F. (1985) "Acoustic Microscopy," *Phys. Today*, **38**, 34-42.

31. Shen, H., Pollak, F.H. (1985) "Raman Study of Polish-Induced Surface Strain in <100> GaAs and InP," *Appl. Phys. Lett.*, **45**, 692-694.

32. Zorabedian, P., Adar, F. (1983), "Measurement of Local Stress in Laser-Recrystallized Lateral Epitaxial Silicon Films over Silicon Dioxide Using Raman Scattering," *Appl. Phys. Lett.*, **43,** 177-179.

Discussion with Reviewers

P. Dhamelincourt: At the end of the section on pulsed laser melting of thin polycrystalline films, some quantitative results have been drawn from the recovery of the amplitude of the line of polycrystalline silicon. Has the author taken into account the possibility that the amplitude should have been influenced by factors other than the absorption coefficient of amorphous silicon i.e., the variation of the roughness of the surface?

Author: This question is very relevant because it is well known that the amplitude of the line may be a rather strong function of the surface roughness. In this particular case, we do not think that surface roughness is a major factor: with respect to Figure 4C, if roughness played a role in region 2, we would actually expect an increase in the amplitude.

P. Dhamelincourt: Could the author discuss in further detail the somewhat surprising long range relaxation phenomenon (revealed by the silicon Raman line recovery) that is observed between the treated (or damaged) material and the virgin one?

Author: This effect does not arise simply from purely mechanical consideration of the relaxation of stress away from a small stressed region of a 1 μm film. We think that this long range effect originates in heating and possibly recrystallization that is not observed of the surface.

B. Wopenka: Does the spot size of the laser depend on the objective used? Was this tested? What were the magnification and numerical aperture of the objective used?

Author: The spot size of the laser depends on the objective used. The work reported here was performed with 40 x magnification and a NA of 0.95. The beam illuminates an area equal to or smaller than 1 μm since we could resolve one micron periodic structures.

B. Wopenka: How do you measure the power at the sample surface? At what power density (W/cm^2) would you expect damage to your samples?

Author: The power is measured at the side entrance of the microscope and 10% of the light actually reaches the sample. Damage with cw focused beams is a strong function of the sample's properties, especially heat conductivity and thickness of the film. We always decrease the laser power down to a level where the Raman line no longer changes with power. This insures that sample heating is insignificant. For these Si films, illuminated in the visible, the power at the sample is 3 mW or less.

B. Wopenka: Several times, the paper refers to different magnitudes of stress in units of $dyne/cm^2$. In a review paper, I would have liked to see an example for the calibration of stress against Raman shifts.

Author: For Si on insulator, the shift is one wavenumber per $2.510^9 dyne/cm^2$ (see for example Ref. 32). For a calibration, see Ref. 1.